Inorganic Chemistry

Article

pubs.acs.org/IC

γ-Brass Polyhedral Core in Intermetallics: The Nanocluster Model

Arina A. Pankova,[†] Vladislav A. Blatov,[†,‡,*] Gregory D. Ilyushin,[§] and Davide M. Proserpio*[,†,⊥]

[†]Samara Center for Theoretical Materials Science (SCTMS), Samara State University, Ac. Pavlov Street 1, Samara 443011, Russia

[‡]Chemistry Department, Faculty of Science, King Abdulaziz University, Jeddah 21589, Saudi Arabia

[§]Institute of Crystallography, Russian Academy of Science, Leninsky Prospekt 59, Moscow 117333, Russia

[⊥]Dipartimento di Chimica, Università degli Studi di Milano, Via Golgi 19, 20133 Milano, Italy

Supporting Information

ABSTRACT: Using the TOPOS program package, 26-atom nanoclusters of the γ-brass (Cu_5Zn_8) type (0@4@22 or 0@8@18) were found in 5918 crystal structures of cubic intermetallics. The nanocluster models were built for all the intermetallics using a recently developed algorithm implemented into TOPOS. The relations of the structures based on the 0@4@22 core are explored as a result of migration of atoms between different shells of the nanoclusters. It is shown that the 0@4@22 nanoclusters frequently occur as building units of intermetallics of different composition and structure type. Regularities in chemical composition of 702 γ-brass-type nanoclusters were found within both the nanoclusters approach (multishell structure) and the nested-polyhedra model. A database containing all topological types of γ-brass nanoclusters is created with which one can search for the corresponding atomic configuration in any intermetallics.

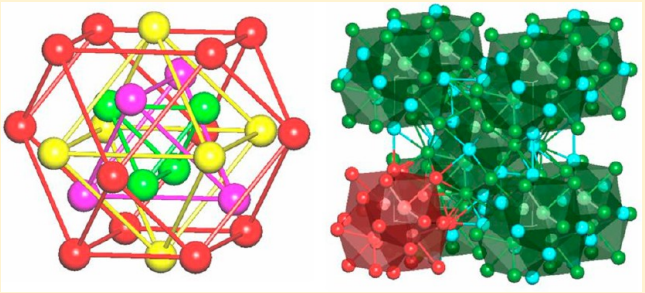

1. INTRODUCTION

In the crystal chemistry of intermetallics, the classification in terms of atomic coordination polyhedra is traditionally used. However, the information about coordination of atoms does not determine the structure as a whole; therefore models that consider building blocks going beyond the first atomic coordination shell have been developed. In intermetallics the best known kinds of building blocks are infinite periodic plane nets[1] as well as finite clusters.[2−6] The cluster models usually treat the structural fragments as nested polyhedra of a regular form that include atoms not necessarily connected to each other. This model has been applied on complicated cubic structures assuming the formation of "empty" or centered (CC) nanoclusters in the high-symmetry positions of the cubic unit cell from a limited set of the nested polyhedra: inner tetrahedron (IT), outer tetrahedron (OT), octahedron (OH), cuboctahedron (CO) and truncated tetrahedron (TT). The set of nested polyhedra does not always include all atoms and bonds of the structure; it usually describes only the general structural motif. In complicated and/or low-symmetrical (not only cubic) structures, the nested polyhedra cannot be selected unambiguously, and as a result, the same intermetallic compound can be described in several different ways.

To resolve these problems, we have proposed the nanocluster method that implements a strict algorithm of searching for the structural units (nanoclusters) that model the entire crystal structure.[7−10] The method was realized in the program package TOPOS[11] and used to explore a number of complex intermetallics,[9,12,13] and the revealed nanoclusters were found in quite different compounds, even belonging to different structure types. In this work, we consider applications of this approach to the intermetallics that belong to the family of γ-brasses. This family is a typical example of a successful application of the nested-polyhedra model. The prototype of the family, *I*-cell γ-brass Cu_5Zn_8 ($D8_2$ in the Strukturbericht notation, space group $I\bar{4}3m$, Pearson symbol *cI*52), in the most common way,[14] is treated as an assembly of 26-atom nested polyhedra clusters (Figure 1 left):

(i) an inner tetrahedron (IT);
(ii) an outer tetrahedron whose vertices are located above the faces of the inner tetrahedron (OT);
(iii) an octahedron whose vertices are projected to the edges of the outer tetrahedron (OH);
(iv) a distorted cuboctahedron with vertices located above the edges of the octahedron (CO).

An alternative description of the *I*-cell γ-brass structure includes four interpenetrating icosahedra whose barycenters coincide with the vertices of the outer tetrahedron (Figure 1 middle), whereas the vertices of the inner tetrahedron fall into the crossing points of three icosahedra.[15] One more known description is based on stella quadrangula[4] with all edges capped (Figure 1 right). The three models are fully equivalent as they completely describe the same structure.[6]

Received: July 30, 2013
Published: October 1, 2013

   dx.doi.org/10.1021/ic4019713 | *Inorg. Chem.* 2013, 52, 13094−13107

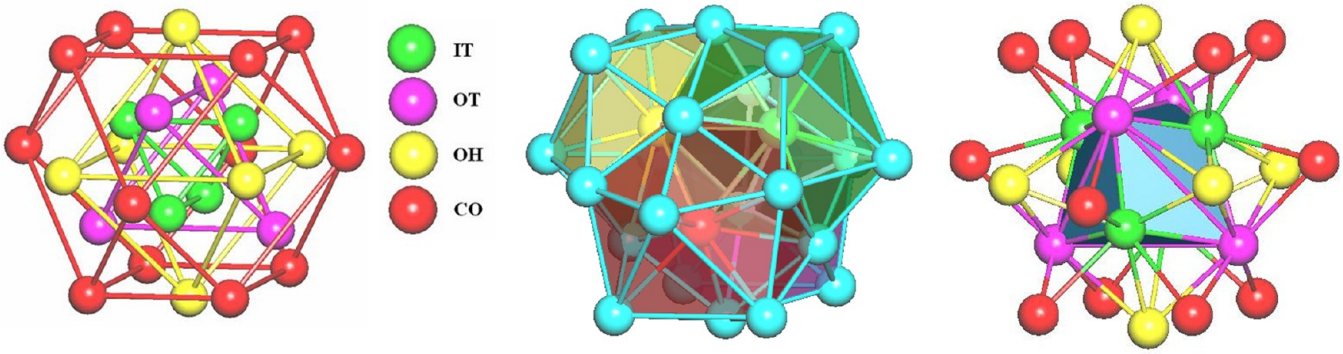

Figure 1. 26-atom γ-brass-type cluster represented (left) as a sequence of polyhedral shells; (middle) as four interpenetrating icosahedra; (right) as stella quadrangular (internal polyhedron) with all 18 edges capped.

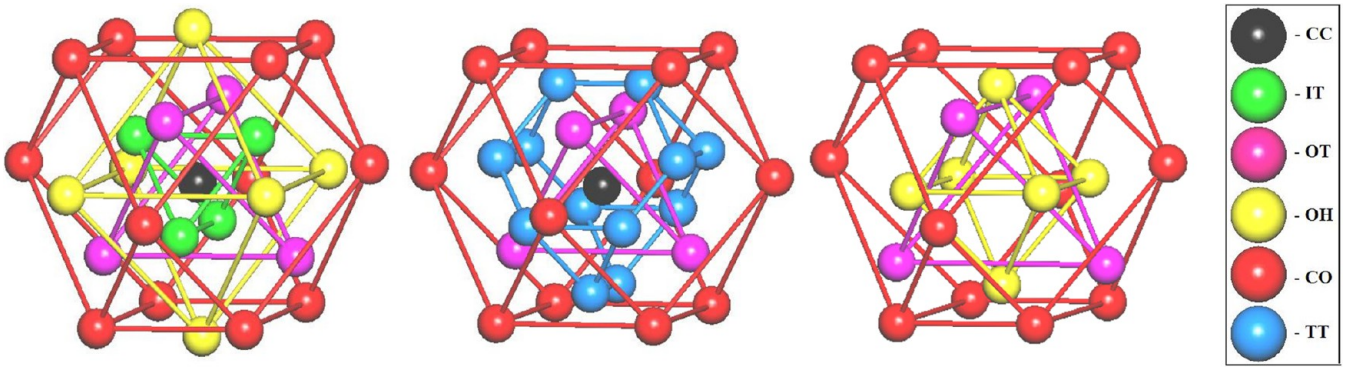

Figure 2. Types of clusters forming the γ'-brass structure: (left) BCC, (middle) α-Mn, (right) Ti_2Ni.

There are symmetry reduced γ-brasses with primitive cubic or rhombohedral cells (P- or R-cell γ-brasses of $P\bar{4}3m$ or $R\bar{3}m$ space-group symmetry, respectively)[16] that contain the same structural units. Other γ-brass related structures with a face-centered cubic cell can be considered as $2 \times 2 \times 2$ superstructures of the I-cell γ-brass and are called F-cell or γ'-brasses; they belong to space group $F\bar{4}3m$.[15−19] In addition to 26-atom cluster (Figure 1 left), there are three other nested polyhedra clusters that form the γ'-brass structures:[3,15] the body-centered cubic (BCC) type (27 atoms, Figure 2 left), the α-Mn type (29 atoms, Figure 2 middle), and the Ti_2Ni type (22 atoms, Figure 2 right).

In this work, we propose a detailed comparison of the nanocluster models of γ-brass and related cubic structures with the models based on the clusters represented as sets of nested polyhedra. We will also discuss the regularities in the chemical composition of the γ-brass-type nanoclusters.

2. EXPERIMENTAL SECTION

To determine the composition and structure of the nanoclusters that assemble intermetallic compounds, we have used the algorithm[11] that is based on the following principles:

(i) The crystal structure presented in the form of a periodic atomic net (i.e., as an ensemble of atoms-nodes and bonds-edges) is formed as a result of a self-assembly of multishell primary nanoclusters corresponding to optimal (fundamental) configurations of atoms. The configurations are assumed to be stable if they occur in different structure types of intermetallics. The primary nanocluster has an "onion" structure which usually contains 1−3 layers. Interconnected centers of the primary nanoclusters form an underlying net which determines the method of the structure assembly (building scheme) from the nanoclusters. Hereafter we use the RCSR bold three-letter codes[20] to designate the underlying net topologies.

(ii) The primary nanoclusters have the highest symmetry in the structure (their centers occupy the most symmetrical positions in the unit cell).

(iii) The primary nanoclusters are usually centered with high-coordinated atoms. However, the nanocluster can be "empty" (noncentered) if they obey the previous principle.

(iv) The primary nanoclusters should not have common internal atoms (i.e., they do not interpenetrate) but they may share their surface atoms. The preferable model (if any) is the so-called packing of primary nanoclusters, where they have no common atoms at all. The packing describes the structure assembly in a simplest way, without eliminating atoms during the assembling of the nanocluster.[21]

(v) The set of primary nanoclusters should include all atoms of the structure. In special cases, single atoms or small groups of atoms (for example, tetrahedral clusters) play the role of filler blocks (spacers), but the number of different spacers should be small.

(vi) The primary nanoclusters condense into supraclusters, which then form microchains. A successive condensation of microchains gives rise to microlayers and finally to a microframework that predetermines the topology of the underlying net.

(vii) If several inequivalent models obey principles (i)−(vi), additional criteria should be applied: the model should be assembled of a minimal number of primary nanoclusters (that is the parsimony or Ockham's Razor principle); the resulting underlying net should have the smallest number of inequivalent nodes and a well-known topology.

Let us consider how this scheme works for I-cell γ-brasses. For all structures of this family described in the literature, first five steps of the nanoclusters approach give three possible models.

(a) A net of two-shell 26-atom noncentered nanoclusters 0@4@22 that coincide with nested clusters in Figure 1. Importantly, the

dx.doi.org/10.1021/ic4019713 | Inorg. Chem. 2013, 52, 13094−13107

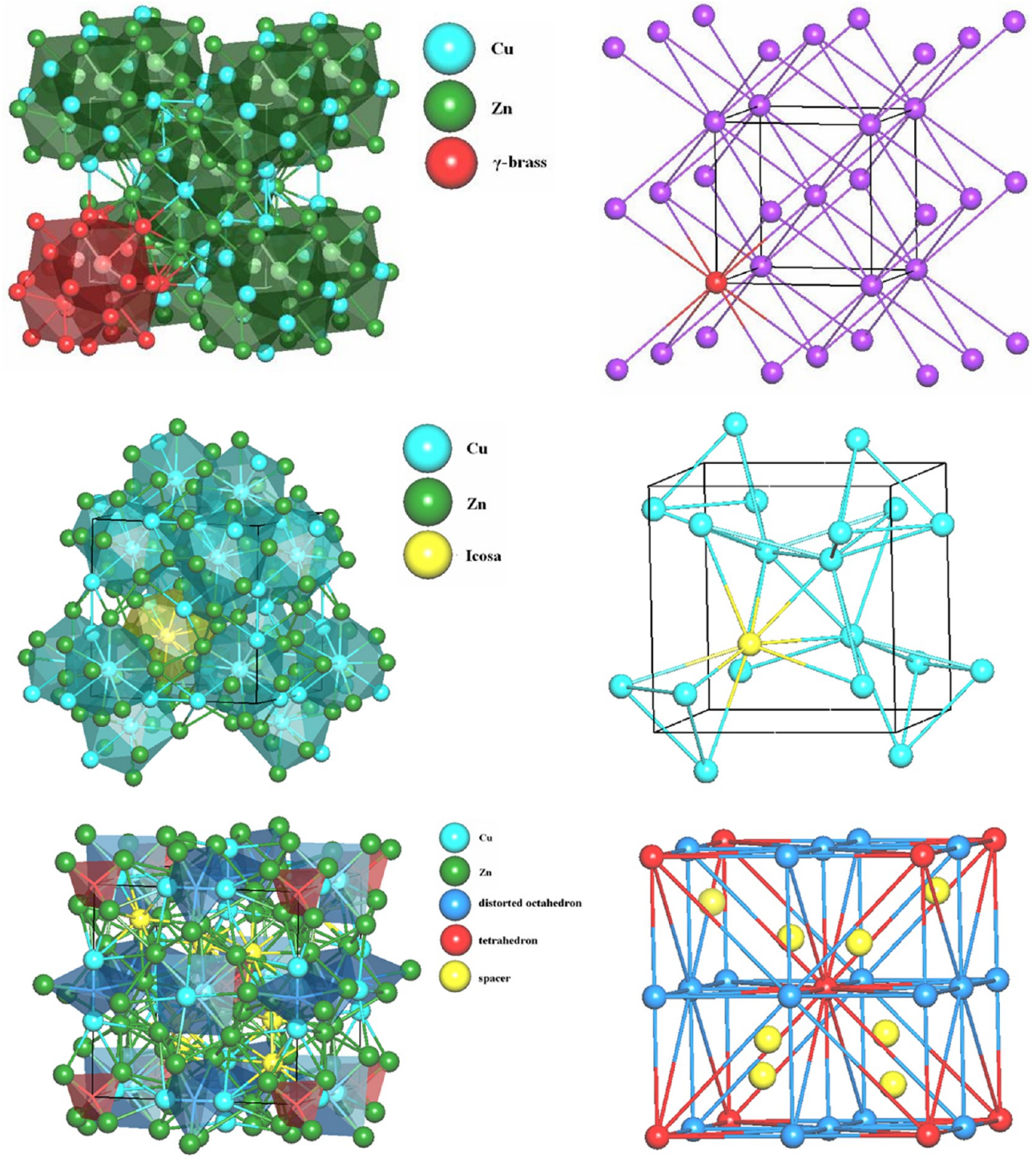

Figure 3. Three nanocluster models for I-cell γ-brass Cu_5Zn_8: nanoclusters (left) and underlying nets (right). (Top) packing of 0@4@22 nanoclusters (additional six contacts of each node are not shown on the right picture for simplicity); (middle) net of icosahedra; (bottom) packing of tetrahedra, distorted octahedra, and spacers.

nanoclusters are obtained irrespective of polyhedral configurations of atoms: the only condition is the shell-by-shell growth according to the connections between atoms. Thus the second 22-atom shell contains all atoms that are in contact with the internal tetrahedral core. These nanoclusters occupy the most symmetrical $\bar{4}3m$ positions and have no common atoms, i.e. form a packing (Figure 3 top left). The corresponding underlying net has the **bcu-x**, which is an extended (8 + 6) = 14-coordination of the body-centered cubic topology (Figure 3, top right).

(b) A net of atom-centered icosahedra 1@12 connected via common vertices and faces (Figure 3 middle left). The central atom of each icosahedron occupies positions $3m$ and shares two faces and all vertices with nine other icosahedra. The resulting underlying net is 9-coordinated **neb** (Figure 3 middle right). In addition, each icosahedron connects 12 other icosahedra by links between their outer atoms; the underlying net is much more complicated and has 9 + 12 = 21-coordinated nodes. This model relates to the description of γ-brass in terms of Pearce clusters[6] or as a packing of condensed icosahedra.[22]

dx.doi.org/10.1021/ic4019713 | *Inorg. Chem.* 2013, 52, 13094−13107

(c) A packing of empty tetrahedra and distorted octahedra in the $\bar{4}3m$ and $\bar{4}2m$ positions, respectively, as well as separate atoms in positions $3m$; these atoms can be considered as spacers (Figure 3 bottom left). The tetrahedra and separate atoms occupy the centers of primary nanoclusters in the previous two models. Each tetrahedron, octahedron, and spacer is connected to 22, 18, and 7 other structural units, respectively, to form a complicated 7,18,22-coordinated underlying net. If we leave the spacer uncoordinated, we get the 10,18-coordinated net illustrated in Figure 3 (bottom right).

Successive application of other conditions of the nanocluster approach allows one to choose model (a) as most preferable. Indeed, this model is better than the second one (b) because it consists of high-symmetry nanoclusters that form a packing. Compared to model (c), it is built with smaller number of nanoclusters and contains no spacers. Sufficiently, this list enumerates all possible methods of decomposing the structure of *I*-cell γ-brass into nonintersecting multishell structural units, so one can choose among the three possible models being sure that no other solutions exist. In this case, as in many other cases, the nanocluster approach leads to a physically reasonable model that was found intuitively without a strict algorithm.[23] However, using the strict algorithm one can process much more complicated crystal structures as well as large samples of crystallographic data in a routine way with the TOPOS package.[7−13]

While any nanocluster always corresponds to a stable atomic configuration, the converse statement is in general incorrect, i.e., not any stable atomic configuration fits all principles of the nanocluster approach. In this case, we call it local atomic configuration. The local atomic configuration is a generalization of the concept of coordination polyhedron; it corresponds to some stable ensemble of atoms to be typical for different structures, but in contrast to coordination polyhedron it concerns not only the nearest environment of a single atom. When the local atomic configuration is constructed according to principle (i), we use the term nanocluster configuration. In this work, we consider only nanocluster configurations.

In this study, we have constructed atomic nets for all cubic as well as some related low-symmetrical intermetallics that are formed only by metal atoms (they are placed below the Zintl line in the Periodic Table) from ICSD (release 2012/2)[24] and Pearson's Crystal Data (version 2010/2011).[25] We have assigned bonds according to the Voronoi-Dirichlet partition with the AutoCN program of TOPOS and took into account the interatomic interactions corresponding to the faces of atomic Voronoi−Dirichlet polyhedra with solid angles no less than 1.5% of 4π steradian. When determining the type of the inner polyhedral core of an "empty" nanocluster (such as 0@4@..., 0@6@..., or 0@8@...), we have considered solid angles of more than 7% for the faces of the Voronoi-Dirichlet polyhedron that was built for the center of the nanocluster. The nanocluster configurations were identified with the algorithm for detecting finite subgraphs of any complexity in infinite periodic graphs; this algorithm has also been implemented into TOPOS.[9] All cubic intermetallic structures that contain the 0@4@22 (Figure.3a) or the related 0@8@18 subgraphs that we call *γ-configurations* were analyzed with the nanoclusters approach.

Totally, we identified 5918 structures of cubic intermetallics containing γ-configuration. Using TOPOS, these intermetallics were arranged in 150 topological types, i.e., groups of structures that have isomorphic atomic nets. The nanocluster models were constructed for one representative of each topological type, because by definition, all the structures belonging to the same topological type are characterized by the same nanocluster model. Note that structures belonging to the same topological type can have different space-group symmetry and, hence, belong to different structure types. This reflects the advantage of the nanocluster model: the description does not depend on any geometrical distortion that does not influence the system of interatomic contacts (topology). On the contrary, geometry plays a crucial role in the nested-polyhedron models, so many of the structures we found were never considered with the nested-polyhedron models. At the same time, topological and structure types of cubic structures usually coincide with each other because the distortions are minor in this case. Therefore we will use the nested-polyhedron models and refer to structure types to show their correlations with the topological description.

For all the nanocluster models, we have catalogued the types of nanoclusters (including the composition, number of layers and the topology of the corresponding graph), constructed the underlying nets and determined their topology. Below we consider in detail those structures that contain γ-configuration as a primary nanocluster or as a part of other two-shell primary nanoclusters. The structures, where γ-configuration is a part of n-shell primary nanoclusters ($n > 2$) or is not included into any primary nanocluster, will be considered in a separate paper.

3. RESULTS AND DISCUSSION

3.1. γ-Configuration in Two-Shell Primary Nanoclusters. The nanocluster analysis of the 150 topological types of intermetallics showed that the 26-atom γ-configuration appears in two-shell noncentered primary nanoclusters of 37 topological types accounting for 576 crystal structures out of 5918. This means that the γ-configuration can be considered as a building block in less than 10% cases. Further we will discuss only those models of the 37 topological types, where primary nanoclusters contain γ-configuration (see Table S1 in the Supporting Information); such nanoclusters usually occupy most symmetrical sites in the structure. We have found three types of internal cores (shells) of these nanoclusters: tetrahedral 0@4, octahedral 0@6, and eight-atom 0@8 where atoms of two nested tetrahedra almost equally surround the central hole forming a distorted cube. These three cores provide different topologies of the second shell and will be considered separately.

3.1.1. Primary Nanoclusters with 0@4 Tetrahedral Core. Two-shell γ-configuration-based primary nanoclusters with inner tetrahedral core can be of two types, 0@4@22 or 0@4@26 (Figures 1, 4). In both cases there are unicluster

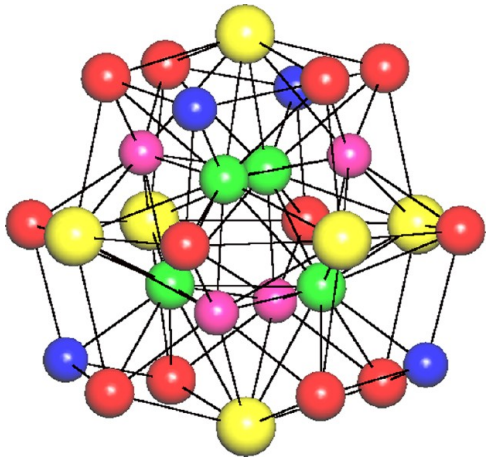

Figure 4. 30-atom primary nanocluster 0@In4@Ce6Pd8In12 (0@4@26) in $Ce_{20}Pd_{36}In_{67}$.[26] The In atoms of IT and CO are highlighted in green and red, respectively, the Ce atoms are yellow and the Pd atoms are magenta. The additional four Pd atoms (blue) are located above the triangular faces of the cuboctahedron.

structures that can be composed of only nanoclusters of one of these types; in other cases such nanoclusters form the structures together with other primary nanoclusters. Evidently, unicluster structures are of special interest within the nanocluster model because they obey Ockham's Razor principle best of all.

dx.doi.org/10.1021/ic4019713 | Inorg. Chem. 2013, 52, 13094−13107

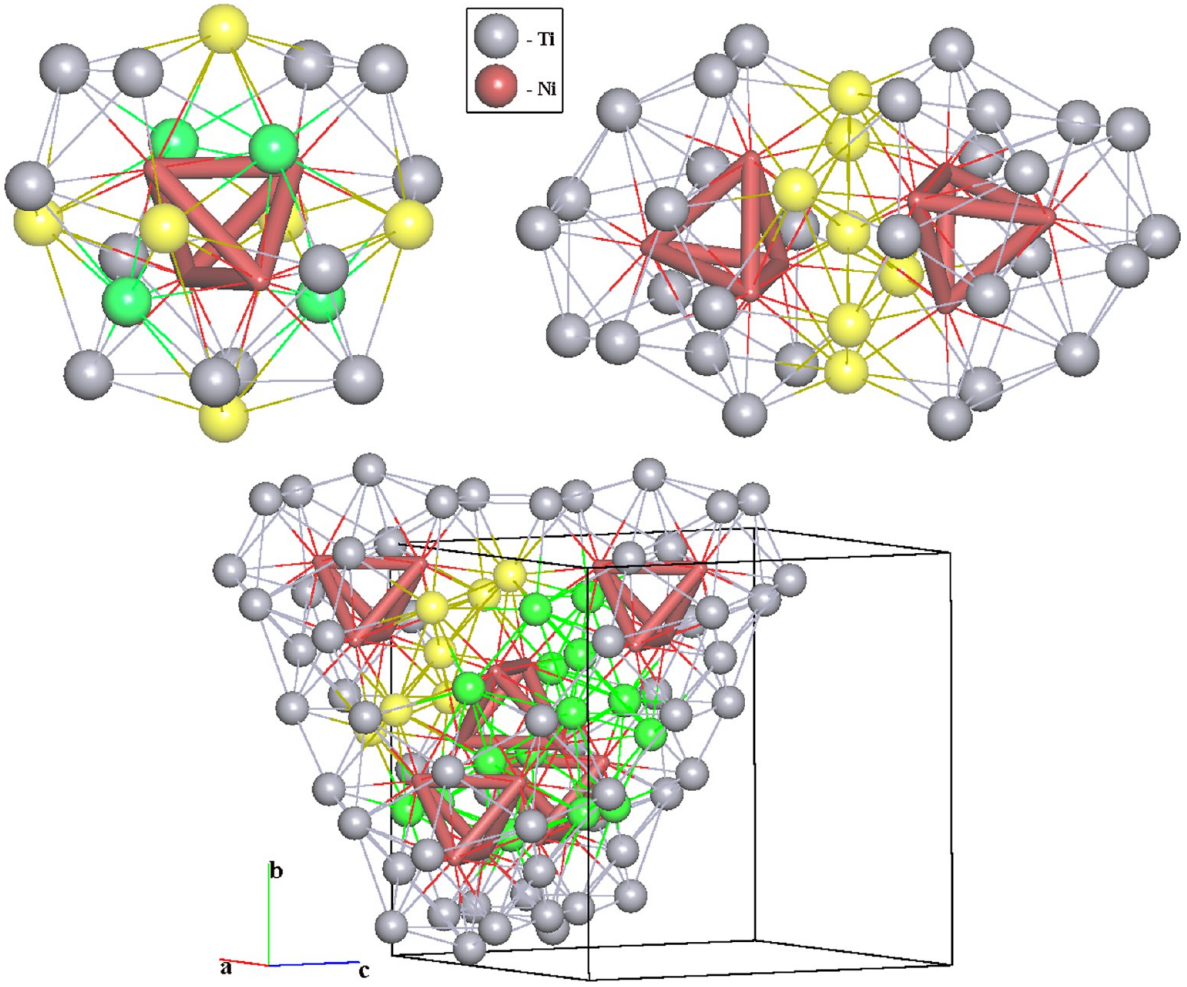

Figure 5. Nanocluster model of Ti_2Ni structure. (Top left): 26-atom γ-brass-type nanocluster 0@Ni4@Ti22; the Ti atoms of OT and OH are highlighted in green and yellow, respectively; (top right): two fused nanoclusters; the common atoms are highlighted in yellow; (bottom): a set of four nanoclusters, which centers form a **dia-x** net; the common atoms of the nanocluster pairs are highlighted in yellow for one pair and in green for other three pairs.

0@4@22 Primary Nanoclusters. These are in fact the clusters that compose *I*-, *P*-, and *F*-cell γ-brasses. The nanocluster models for *I*-cell γ-brass were considered above (Figure 3); *P*-cell and *F*-cell γ-brasses contain two or four symmetry independent 0@4@22 nanoclusters, but the main building scheme for them is the same: the nanoclusters form a packing with the extended body-centered cubic 14 coordinated **bcu-x** underlying net topology. In some cases, there can be spacers embedded into the **bcu-x** packing of γ-brass-type nanoclusters. Thus, in the $Ba_5Ti_{12}Sb_{19.10}$ crystal structure[27] there is a **sod** (sodalite-like) network of Ti and Sb atoms, which are allocated inside the cavities of the **bcu-x** packing of 0@4@22 nanoclusters.

Another method of connecting 0@4@22 nanoclusters was revealed in the structures of the Ti_2Ni structure type (space group $Fd\bar{3}m$). Following Chabot, Cenzual, and Parthé,[3] the Ti_2Ni structure is traditionally considered as a packing of 22-atom Ti_2Ni-type clusters (Figure 2 right), although the γ-brass cluster is also mentioned.[3] Indeed, the first visual representation of the structure[28] contains a part of γ-brass cluster, but the authors do not mention it. The nanocluster approach unambiguously gives a model where Ni_4-based γ-brass-type nanoclusters (see Table S1 in the Supporting Information; Figure 5, top left) are fused sharing seven atoms (Figure 5, top right). Each nanocluster of this type is in close contact with four other nanoclusters (Figure 5, bottom) and with 12 more distant ones to form an extended diamond coordination 4 + 12 = 16 (**dia-x**) underlying net. Octahedron-based nanoclusters of the Ti_2Ni type are forbidden in the nanocluster model according to the structure connectivity; they should have 40 atoms over the octahedral core (not 16 as in the Ti_2Ni cluster) and would interpenetrate to each other. This conclusion emphasizes the difference between the nanocluster and nested-polyhedra approaches: the nanocluster model takes into account contacts between atoms and pays no attention to their spatial arrangement.

One more topology of the underlying net of 0@4@22 nanoclusters occurs in the $Mn_5Ni_2Bi_4$ crystal structure (space group $F\bar{4}3m$).[29] In this case, the Mn atoms composing the cuboctahedron are not in contact to each other (Figure 6 left), but all of them are connected to the central Mn_4-tetrahedron. Each of the nanoclusters shares the 12 external Mn atoms with 12 other nanoclusters that leads to a face-centered cubic (**fcu**) underlying net. Two nonequivalent Bi atoms (Bi2 and Bi3) lie outside the second shell of nanocluster playing the role of spacers (Figure 6 right). The authors[29] talk about local similarity of tetrahedral positions to metallic manganese, but do not consider the cluster representation.

dx.doi.org/10.1021/ic4019713 | *Inorg. Chem.* 2013, 52, 13094−13107

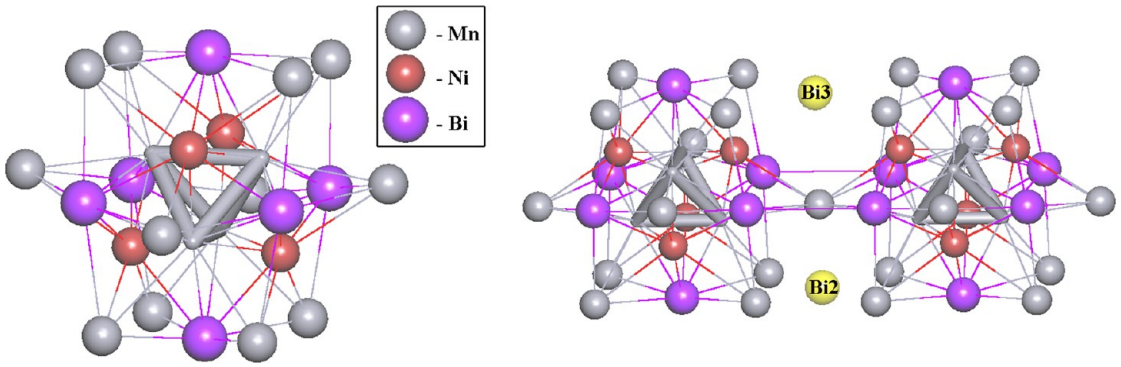

Figure 6. 26-Atom γ-brass-type nanoclusters in $Mn_5Ni_2Bi_4$. (Left) 0@Mn4@Ni4Bi6Mn12 nanocluster; (right) two nanocluster sharing one Mn atom and two Bi spacers.

Another example of the **fcu**-type arrangement of 0@4@22 nanoclusters is the large group of 72 structures of the Gd_4RhIn type (space group $F\bar{4}3m$).[30] In this case, the In_4-based nanoclusters (Figure 7 left) are also merged by one common atom

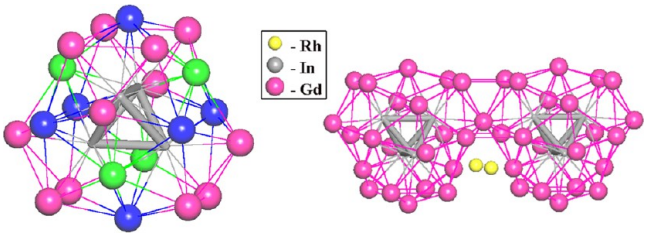

Figure 7. 26-Atom γ-brass-type nanoclusters in Gd_4RhIn. (Left) 0@In4@Gd22 nanocluster; the Gd atoms of OT and OH are highlighted in green and blue, respectively; (right) two nanocluster sharing one Gd atom and two Rh spacers.

(Figure 7 right). The structures of $Mn_5Ni_2Bi_4$ and Gd_4RhIn are hence topologically similar that is also reflected by correspondences in atomic positions. The only difference is in the orientation of the γ-brass-type nanoclusters as well as in the number and positions of spacers (Table 1).

Table 1. Positions of Atoms in $Mn_5Ni_2Bi_4$[29] and Gd_4RhIn[30] and Their Role in the Nanocluster Models

$Mn_5Ni_2Bi_4$	Gd_4RhIn	Wyckoff position	position in the nanocluster
Mn(1)	In	16*e*	IT
Ni	Gd(3)	16*e*	OT
Bi(1)	Gd(2)	24*f*	OH
Mn(2)	Gd(1)	24*g*	CO
Bi(2), Bi(3)		4*c*, 4*d*	spacers
	Rh	16*e*	spacer

The last way of assembling 0@4@22 nanoclusters is realized in another rich (236 representatives) structure type of Th_6Mn_{23}.[31] In this case, the nanoclusters (Figure 8 top left) are fused via five atoms and their internal tetrahedra are oriented to each other by edges (Figure 8 top right). This method differs from the fusion in Ti_2Ni (Figure 5) and results in the **pcu** underlying net, which occurs in α-Po (Figure 8 bottom). Note that Nyman[32] described the γ-brass-type nanoclusters in Sr_6Mg_{23} that belongs to this structure type.

In the crystal structure of $Al_{7.56}Pd_{18.0}Zn_{74.44}$, the fourth $\bar{4}3m$ position is occupied by another nanocluster 0@4@30 that in terms of nested polyhedra can be described with the sequence IT+OH+CO+TT (Figure 9 left); the ratio of the 0@4@22 and 0@4@30 nanoclusters is 3:1. The authors[15] consider this cluster as of γ-brass type with vacant OT, but the nanocluster approach allows one to interpret the structure model in another way, as a kind of 0@4 nanocluster. Note that another structure, Pt_3Zn_{10},[33] where one γ-brass-like cluster has vacant OH positions, was not confirmed by a latter investigation.[34]

The $\bar{4}3m$ positions in the crystal structure of $Li_{13}Na_{29}Ba_{19}$[35] are occupied by two 0@4@22 nanoclusters (Li_4Li_{22} and $Na_4(Na_6Ba_{16})$) and two Ba-centered Friauf polyhedra $Ba(Ba_4Na_{12})$. The nanocluster model is completed with sodium-centered icosahedral spacers. The authors talk about new pure lithium γ-brass-type cluster, however, according to our analysis of chemical composition of nanoclusters (see below) such Li_4Li_{22} nanocluster exists also in the $Li_{10}Pb_3$ γ-brass.[36] In $Ce_{20}Mg_{19}Zn_{81}$,[37] two positions of the tetrahedron symmetry are occupied by Mg-centered Friauf polyhedron $Mg(Ce_4Zn_{12})$ and Zn-centered cube $Zn(Zn_8)$. At last, in $Ce_{20}Pd_{36}In_{67}$[26] one 0@4@22 nanocluster is combined with two 0@4@26 nanoclusters; this structure is considered in the next part.

0@4@26 Primary Nanoclusters. The 0@4@26 primary nanocluster can be considered in the nested-polyhedra approach as IT+OT+OH+CO+ET where ET designates external tetrahedron, which vertices are projected to triangular faces of CO and directly connected to the vertices of IT (Figure 4). In the nanocluster approach, this type of nanocluster appears naturally because the bonds IT−ET are often even stronger than other bonds between atoms of the second shell and internal core. For example, in the cited above $Ce_{20}Pd_{36}In_{67}$,[26] the contacts In−Pd that correspond to the IT−ET bonds are the shortest for In atoms. In all cases the 0@4@26 nanoclusters coexist with other γ-brass-like nanoclusters (see Table S1 in the Supporting Information).

3.1.2. Primary Nanoclusters with 0@6 Octahedral Core. In superstructural *P*-cell or *F*-cell γ-brasses, the γ-brass-type nanocluster can coexist with other two-shell nanoclusters. In such cases, its most typical "neighbor" is the nanocluster 0@6@28, which includes the 22-atom Ti_2Ni cluster (Figure 2 right) as a subgraph (Figure 9 right). This 34-atom nanocluster is an "isomer" of 0@4@30, which was mentioned in the previous part; the 0@6@28 and 0@4@30 nanoclusters can be transformed to each other by reversing inner octahedron and tetrahedron. The **bcu-x** underlying net describes assembling the structure of Cd_5Ni (space group $P\bar{4}3m$) with a combination 0@4@22 + 0@6@28 and this description coincides with the model proposed in the original paper,[38] but the authors use

dx.doi.org/10.1021/ic4019713 | *Inorg. Chem.* 2013, 52, 13094−13107

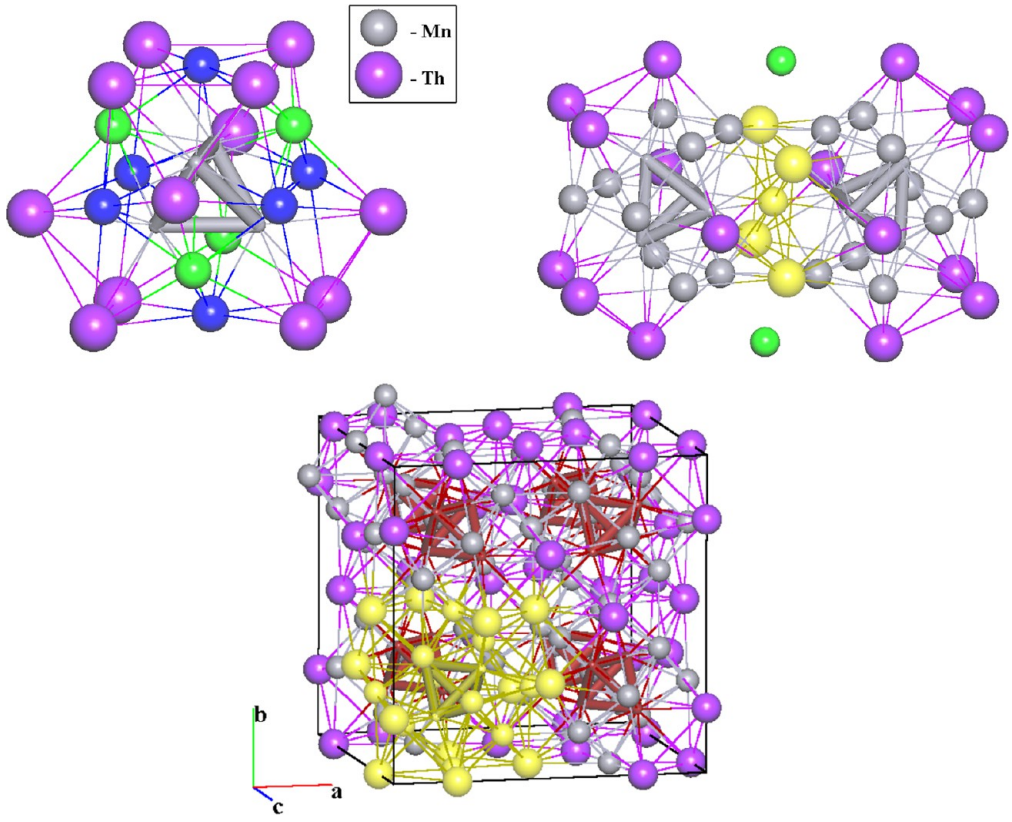

Figure 8. Nanocluster model of Th_6Mn_{23} structure. (Top left) 26-atom γ-brass-type nanocluster 0@Mn4@Mg10Th12; the Mg atoms of OT and OH are highlighted in green and blue, respectively; (top right): two fused nanoclusters; the common atoms and spacers are highlighted; (bottom) a set of eight nanoclusters, which centers form a **pcu** net; one nanocluster is highlighted.

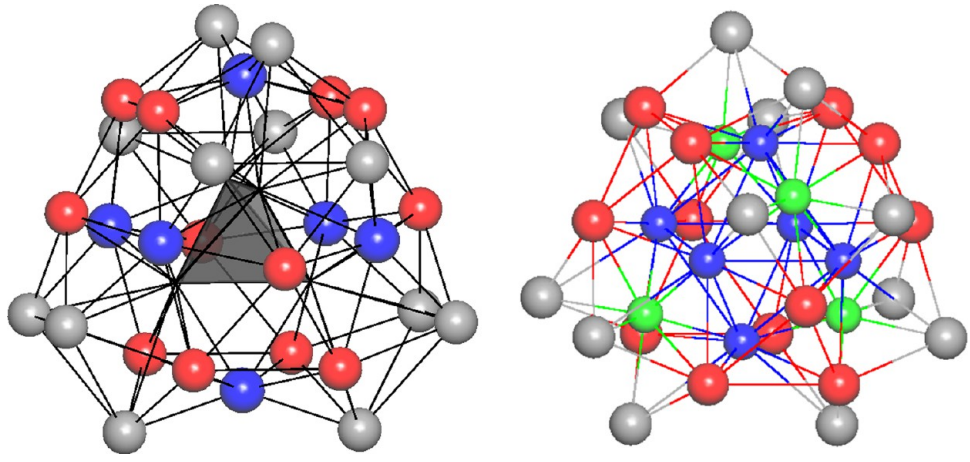

Figure 9. (left) 0@Al4@Pd6Zn24 (0@4@30) nanocluster in $Al_{7.56}Pd_{18.0}Zn_{74.44}$; the Zn atoms of OH, CO, and TT are highlighted in blue, red and gray, respectively; (right) the relation between 0@6@28 and Ti_2Ni nanoclusters: the atoms of OH, OT, and CO of the Ti_2Ni nanocluster are highlighted in blue, green, and red, respectively; twelve additional TT atoms of the 0@6@28 nanocluster are gray.

Ti_2Ni cluster instead of 0@6@28. Twelve additional atoms form truncated tetrahedron (TT) above the Ti_2Ni cluster and their distances to the octahedron vertices are even smaller than the distances inside the octahedron (Figure 9 right). Thus the nanocluster 0@6@28 can be considered as an analogue of the Ti_2Ni cluster in the nanocluster model. Importantly, both nanocluster and the authors' models give the same body-centered cubic motif of the cluster assembling, i.e., the differences between two models are unessential.

The crystal structure of β-$Al_{67.4}Cu_{14.3}Cr_{18.3}$[39] is similar to Cd_5Ni, but here the space group is $F\bar{4}3m$ and the ratio of 0@4@22 and 0@6@28 clusters is 2:1 (they occupy three of four positions with the tetrahedron symmetry $\bar{4}3m$, moreover, in the remaining $\bar{4}3m$ position, there is spacer $Cu(Cu_{12}Al_4)$ in the form of a Friauf polyhedron. The authors[39] do not consider this model. At last, the ratio 3:1 is observed in the $Mg_{44}Rh_7$[40,41] and Na_6Tl[42] crystal structures.

Another octahedron-based nanocluster, 0@6@32, is observed in $Ce_3Ge_{10.72}Pt_{23.28}$.[43] The outer shell of this nanocluster can be treated as EC+TO (Figure 10 left), where EC designates external cube, and TO is a 24-vertex truncated octahedron. The third type of the second shell occurs in Mg_6Pd;[44] the shell

dx.doi.org/10.1021/ic4019713 | Inorg. Chem. 2013, 52, 13094−13107

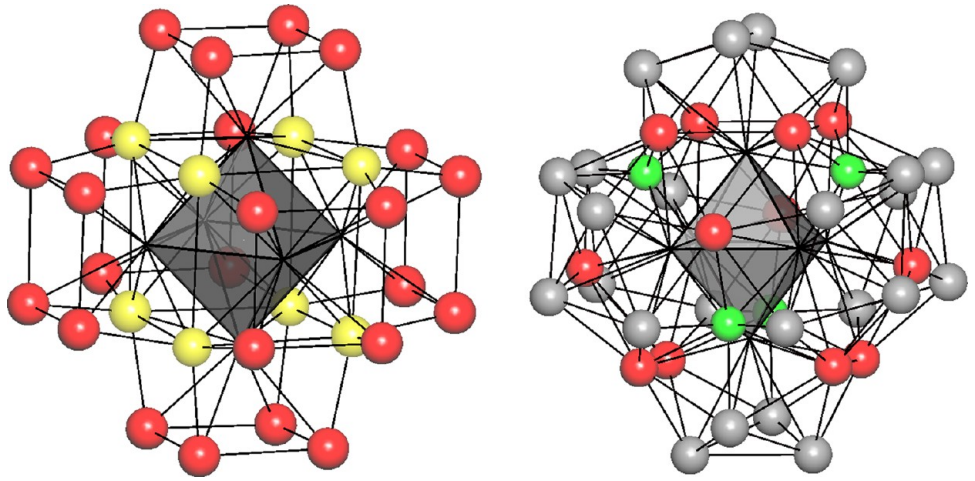

Figure 10. Two-shell nanoclusters with octahedral core: (left) 0@Pt8@Ge4Pt28 (0@6@32) in $Ce_3Ge_{10.72}Pt_{23.28}$ and (right) 0@Mg6@Mg36Pd4 (0@6@40) in Mg_6Pd; Pd atoms of OT and Mg atoms of CO are green and red, respectively.

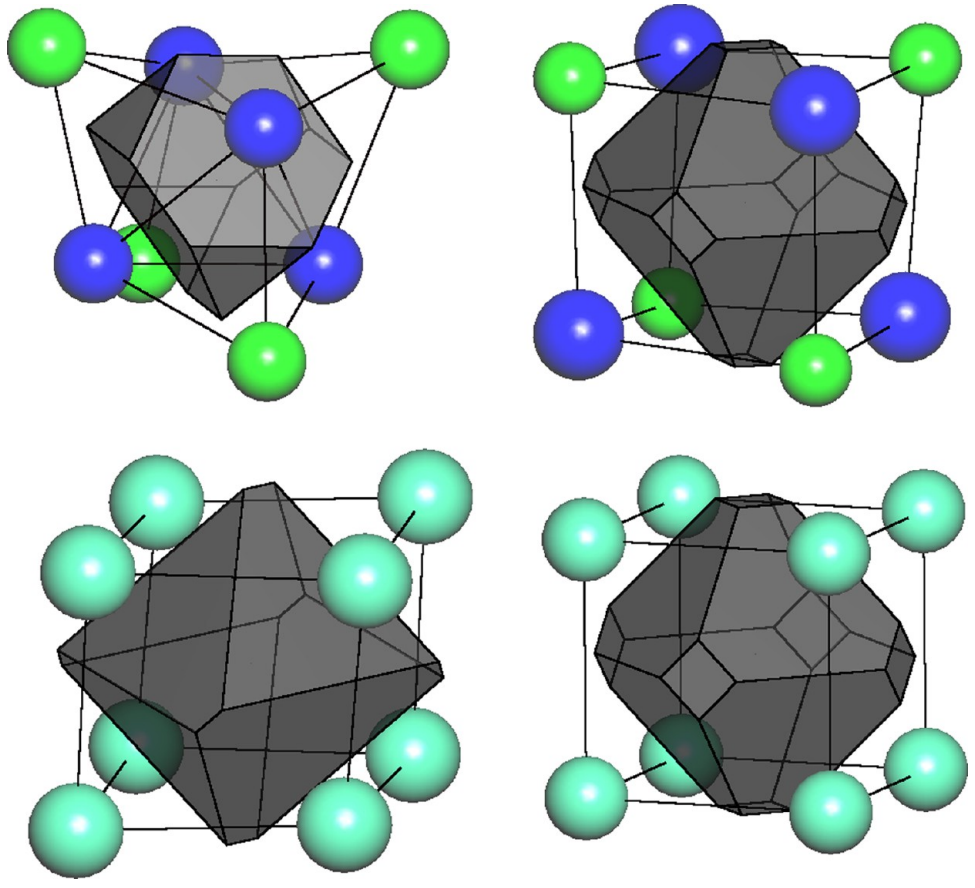

Figure 11. 0@8 cavities represented as Voronoi polyhedra in (top) Zn_4Cu_4 in Cu_5Zn_8[45] and Na_4Sn_4 in $Ba_{16}Na_{204}Sn_{322.38}$;[46] (bottom) Cd_8 in Ce_6Cd_{37}[47] and Ga_8 in $TmRuGa_3$.[48]

contains 40 atoms, of which only 16 can be assigned to nested polyhedra OT+CO that indicates the Ti_2Ni cluster. The remaining 24 gray atoms in Figure 10 right follow a strongly distorted TO or TT+TT motif.

3.1.3. Primary Nanoclusters with 0@8 Core. The primary nanoclusters based on the 0@8 core can exist in the form of two nested tetrahedra or a regular or slightly distorted cube. The structures that contain such nanoclusters are not the Hume–Rothery phases but have relations to them at the nanocluster level. To show such relations one can use the representation of the hole in the nanocluster center as Voronoi polyhedron (Figure 11). A typical γ-brass configuration IT+OT has clear differences between sizes of the Voronoi polyhedron faces corresponding to the nested tetrahedra: for Cu_5Zn_8[45] the solid angles (Ω) of hexagonal and trigonal faces corresponding to IT and OT vertices are 21.3 and 3.7% of 4π steradian, respectively (Figure 11 top left). Another type of the 0@8 core can be treated as an intermediate form between the pair

dx.doi.org/10.1021/ic4019713 | *Inorg. Chem.* 2013, 52, 13094–13107

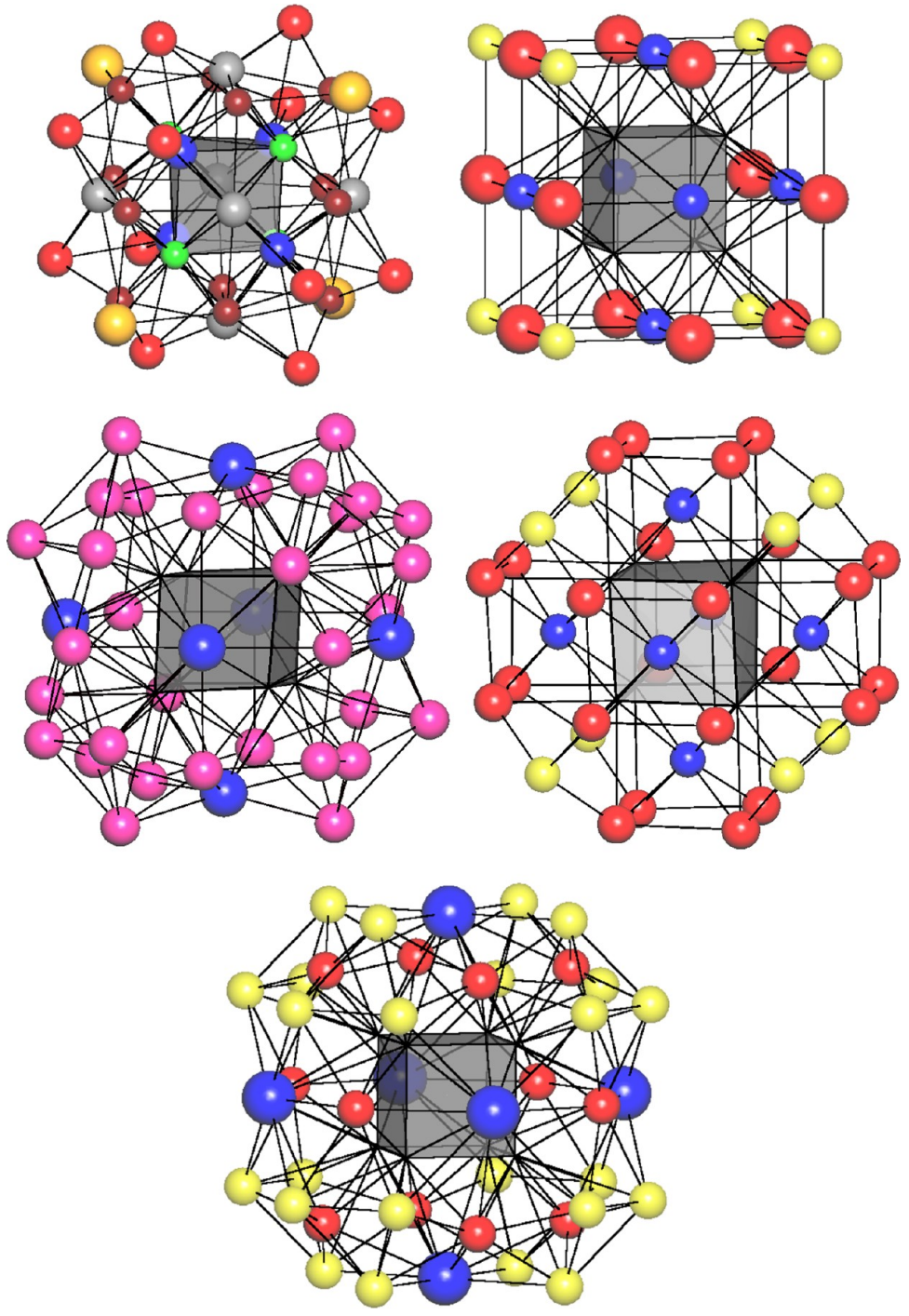

Figure 12. Two-shell nanoclusters: (top) 0@Sn4Na4@Ba4Na18Sn12 (0@8@34) in $Ba_{16}Na_{204}Sn_{322.38}$ (OH, CO, TT, and ET atoms are colored in gray, brown, red, and yellow, respectively) and 0@Ga8@Tm12Ga8Ru6 (0@8@26) in $TmRuGa_3$ (OH, CO, and EC atoms are colored in blue, red, and yellow, respectively); (middle) 0@8@38 in Ce_6Cd_{37} (0@Cd8@Cd32Ce6) and $Ce_3Ge_{10.72}Pt_{23}$ (0@Pt8@Ge14Pt24, OH, EC, TO atoms are colored in blue, yellow, and red, respectively); (bottom) 0@Hg8@Ba6Hg36 (0@8@42) in $BaHg_{11}$ (OH, CO, and TC atoms are colored in blue, red, and yellow, respectively).

IT+OT and regular cube. We found this type only in $Ba_{16}Na_{204}Sn_{322.38}$;[46] in this case Ω(IT) = 13.7% and Ω(OT) = 10.2% and the two tetrahedra can be considered as a distorted cube (Figure 11, top right). Another kind of distortion is observed in Ce_6Cd_{37}:[47] the cube is slanted no reason to separate any tetrahedron in this case (Figure 11 bottom, left). At last, in the $TmRuGa_3$[48] and $BaHg_{11}$[49] structure types there are regular cubes and the hole is represented by a regular Voronoi polyhedron too (Figure 11 bottom right). If we consider the IT+OT combination as a whole, the second type of the 26-atom γ-configuration, 0@8@18 can be treated. Table S1 in the Supporting Information shows that all 0@8@*N* nanoclusters have $N > 18$; however, all of them contain the 0@8@18 subgraph and hence are studied in this paper.

As follows from Figure 11, three types of two-shell 0@8@*N* nanoclusters are formed. In $Ba_{16}Na_{204}Sn_{322.38}$ the second shell contains 34 atoms that can be described in terms of nested polyhedra as a sequence OH+CO+TT+ET, where TT and ET

dx.doi.org/10.1021/ic4019713 | *Inorg. Chem.* 2013, 52, 13094−13107

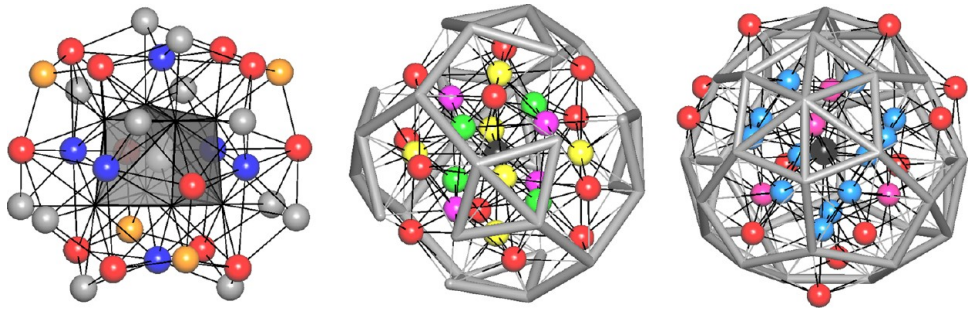

Figure 13. Two-shell nanoclusters: (left) Zn@Zn8@Ir4Zn30 (1@8@34) in $Ir_{7+7\delta}Zn_{97-11\delta}$ (OH, CO, TT and ET atoms are colored in blue, red, gray, and yellow, respectively); (middle) Fe@Fe10Zn4@Zn40 (1@14@40) in $(FeNi)Zn_{12.7}$ (IT, OT, OH, and CO atoms are colored in green, magenta, yellow, and red, respectively); (right) Na@Cd16@Cd20Na24 (1@16@44) in $NaCd_2$ (tetrahedron, TT, and CO atoms are colored in magenta, light blue, and red, respectively).

are truncated tetrahedron and external tetrahedron (Figure 12, top left). TT and ET are composed of Na and Ba atoms, respectively, while internal polyhedra OH and CO consist of Na and Sn atoms. The same type of nanocluster occurs in Ti_8In_5.[50] Second shells of the nanoclusters in $TmRuGa_3$ and Ce_6Cd_{37} contain 26 and 38 atoms, respectively. For $TmRuGa_3$ the sequence OH+CO+EC can be proposed (Figure 12, top right). This nanocluster can be considered as a fragment of NaCl structure where the central atom is replaced by a cube. Nested-polyhedra approach does not work properly for Ce_6Cd_{37} because of distortion of the second shell (Figure 12, middle left), however, almost regular 0@8@38 configuration exists in $Ce_3Ge_{10.72}Pt_{23.28}$;[43] the 38 atoms form an OH+EC+TO (Figure 12, middle right). $Ce_3Ge_{10.72}Pt_{23.28}$ also contains 0@4@26 and 0@6@32 nanoclusters, which were discussed above; the total sequence of nested polyhedra in the 0@6@32 nanocluster, OH+EC+TO, formally coincide with that on the second shell of the 0@8@38 nanocluster. At last, in $BaHg_{11}$, the nanoclusters have 42 atoms in the second shell that correspond to the sequence OH+CO+TC, where TC is a 24-atom truncated-cube configuration (Figure 12, bottom). Both in $TmRuGa_3$ and in $BaHg_{11}$ the nanoclusters are packed according to α-Po (**pcu**) motif that exists also in NaCl, but in $BaHg_{11}$, there are additional Hg spacers.

3.2. Centered Primary Nanoclusters. Besides empty nanoclusters, the nanocluster models of γ-brasses can include centered (−CC) nanoclusters that relate to the γ-configuration-based nanoclusters described above.

In the $Ir_{7+7\delta}Zn_{97-11\delta}$ phases, there is a two-shell centered 1@8@34 nanocluster that contains the BCC cluster (Figure , left) as a subgraph (Figure 13, left). As in the case with the pair 0@6@28 − Ti_2Ni, the 1@8@34 nanocluster can be considered as an analogue of the BCC cluster in the nanocluster approach. Compared to the BCC cluster, 1@8@34 has 16 additional atoms arranged over vertices of a TT and an ET (Figure 13, left). This model coincides with description of the structures of $Ir_{7+7\delta}Zn_{97-11\delta}$ phases in the original paper.[51]

The structure of $(FeNi)Zn_{12.7}$[52] contains the primary nanocluster 1@14@40, which can be treated as containing a centered γ-configuration 1@(IT+OT+OH)@CO that is "wrapped" into a 28-atom shell of Zn atoms (Figure 13, middle; cf. Figure 1, left).

The other centered nested-polyhedron cluster of the α-Mn type (Figure 2 middle) can be formally separated in one of the primary nanoclusters of $NaCd_2$, 1@16@44, that we described earlier.[12] Indeed, the 16 atoms of the first shell can be considered as a combination of nested tetrahedron and truncated tetrahedron, whereas 12 atoms of the second shell form a distorted cuboctahedron (Figure 13 right). Other 32 atoms of the second shell fill the gaps between the CO atoms. This description demonstrates how the nested-polyhedron model become unreasonable if one does not take into account the connectivity of the atoms. Obviously, the nanocluster model is more appropriate in this case.

3.3. Comparative Analysis of the Nanocluster and Nested-Polyhedra Models. The analysis of nanoclusters shows that in many cases they can be associated with the clusters consisting of nested polyhedra. The nested-polyhedron approach is useful to understand the relations between different nanoclusters (Scheme 1). In terms of nested polyhedra these

Scheme 1. Relations between γ-Brass-Type Nanoclusters

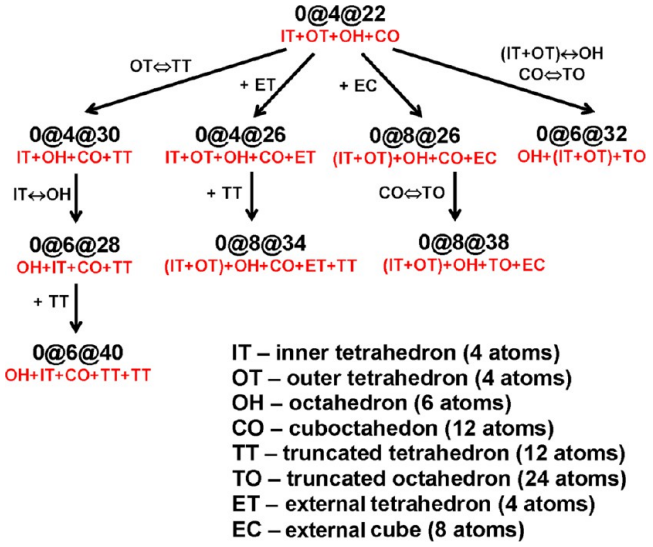

relations are manifested in three kinds of operation: (i) "↔" exchanging some nested polyhedra in the sequence; (ii) "⇔" extending/shrinking a nested polyhedron; (iii) "+" adding a nested polyhedron. In Scheme 1, these operations are designated by the "↔", "⇔', and "+" symbols, respectively. The γ-configuration 0@4@22 serves as a template to obtain more complicated two-shell nanoclusters with the three operations.

In most cases, the nanocluster models are similar to the traditional models based on clusters in the form of nested polyhedra. The results of comparative analysis of these models (see Table S2 in the Supporting Information) reveal the following types of similarity:

dx.doi.org/10.1021/ic4019713 | Inorg. Chem. 2013, 52, 13094−13107

(i) For *I*-, *P*-, and *F*-cell γ-brasses as well as for the $Sr_{11}Ir_4$ structure type the nested-polyhedra model and one of the nanocluster models lead to the same results.

(ii) A partial similarity of the models of the crystal structures, when the cores of the clusters are the same, is observed in 12 topological types. In seven cases, the difference is inessential and typically consists in that the nanocluster model considers some atoms of the outer shell to be shared between nanoclusters, while nested-polyhedron model attributes them to one cluster. Thus, both authors' and nanocluster models represent the structure of Cd_5Ni[38] as a combination of γ-brass and Ti_2Ni-core clusters that form a **bcu-x** underlying net (see Table S2 in the Supporting Information). The difference is that in the nanocluster model the Ti_2Ni core is surrounded by additional Cd5 atoms (Table 2, Figure 14) that are located in the vertices of the nested truncated tetrahedron, i.e., the corresponding nanocluster is 34-atom 0@6@28 and can be represented as (OH+OT+CO)+TT. The Cd5 atoms are attributed to the nanocluster 0@6@28 in accordance with principle (i) of the nanocluster approach since they are connected to atoms of the first shell (OT). However, this difference is unessential because the atoms Cd5 in the nanocluster model are shared between the nanoclusters 0@6@28 and 0@4@22.

In the remaining five topological types, the nanoclusters include a core of only one of the authors' clusters. Thus, the nanocluster model of Gd_4RhIn consists of one type of the 0@4@22 clusters (see above) arranged over a **fcu** underlying net, the holes of which are filled with Rh spacers, whereas the authors' model[30] includes three polyhedra: triangular prism $RhCd_6$, tetrahedron In_4, and octahedron Gd_6 (Figure 15). A more recent work[53] on Gd_4RhIn-like intermetallics finds γ-brass units that supports the nanocluster model.

(iii) In 13 structure types, the authors separated structural units that significantly differ from nanoclusters because the units are allocated in other positions and not based on γ-brass clusters. For a number of intermetallic structures, several completely different cluster models are known. Thus, Samson and Hansen[42] found 14 different icosahedra and 42 pentagonal prisms in Na_6Tl; four icosahedra are fused through their faces and edges to form a 98-atom cluster (see Table S2 in the Supporting Information), which center occupies 4*a* positions. The unit cell contains four such clusters of 392 atoms in total. Then they identified truncated tetrahedra located in 4*a* positions that are shared among the four 98-atom clusters. An alternative description of the Na_6Tl crystal structure[51] includes four clusters relating to three types: γ-brass, α-Mn (−CC), and Ti_2Ni. The nanocluster model corresponds to the latter description, but the Ti_2Ni−core nanocluster includes additional 12 Na4 atoms like in Cd_5Ni (Figure 16).

(iv) Authors of the original papers have not proposed any cluster model for seven structure types under consideration.

This comparison shows that the nanocluster model allows one to find the γ-configurations in the structures where the traditional geometrical approach becomes ambiguous or gives no appropriate model. If the γ-brass clusters are regular, the nanocluster model naturally reflects the connectivity between atoms of nested polyhedra and coincides with the geometrical model. However, even in cubic intermetallics, the structures with rather irregular environment of the cluster centers emerge that can hardly be described with the nested polyhedra.

3.4. Database on γ-Brass-Type Nanoclusters. An important advantage of the nanocluster approach is that the information on the nanocluster topology can be stored as a computer file and then used to search through the electronic databases. We have created a database with all the γ-brass-type nanoclusters described in this paper; the full data on the nanocluster topology are represented in a set of 28 TOPOS-readable *gph*-format files. Each *gph* file has a name of the

Table 2. Models of the Cd_5Ni Crystal Structure

	authors' model[38]		nanocluster model	
nested polyhedra	Ti_2Ni cluster (0,0,0)	γ-brass cluster (1/2, 1/2, 1/2)	nanocluster 0@6@28 (0,0,0)	nanocluster 0@4@22 (1/2, 1/2, 1/2)
IT		Cd1		Cd1
OT	Ni1 + Cd6	Cd2	Ni1 + Cd6	Cd2
OH	Ni2 + Cd7	Cd3	Ni2 + Cd7	Cd3
CO	Cd4	Cd5	Cd4	Cd5
TT		Cd5		

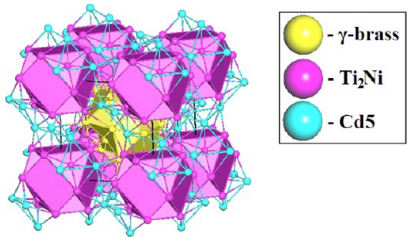

Figure 14. Assembly of 26-atom 0@4@22 (γ-brass) and 34-atom 0@6@28 (Ti_2Ni-based) primary nanoclusters that form a **bcu-x** underlying net in the Cd_5Ni structure.

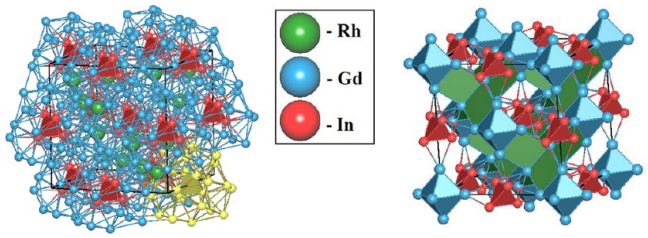

Figure 15. Assembly of the Gd_4RhIn structure: (left) with γ-brass clusters and Rh spacers (the nanocluster model); (right) with triangular prisms, tetrahedra and octahedra.[30]

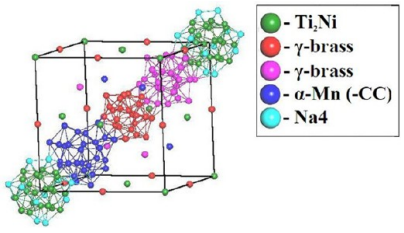

Figure 16. Assembly of Ti_2Ni, γ-brass and α-Mn (−CC) clusters in the Na_6Tl structure.

dx.doi.org/10.1021/ic4019713 | *Inorg. Chem.* 2013, 52, 13094−13107

corresponding two-shell nanocluster; using the TOPOS procedure of searching for a finite atomic fragment we have found all (not only cubic) intermetallics that are stored in ICSD or Pearson's Crystal Data and contain any of the nanocluster configurations from the database. The results are summarized in Table 4; one can see that the 0@4@22 γ-configuration is rather frequent in low-symmetrical intermetallics as well. The search for clusters of nested polyhedra can also be performed if one takes into account their relations to γ-configurations (Table 4). Recall that in low-symmetrical intermetallics, the nested-polyhedron description may be formal or not applicable at all; in such cases, the nanocluster approach becomes most important.

Table 3. Composition of Shells in A_4B_{22} γ-Brass Nanoclusters

A	B	structures
Mg	Ca, Ce, Dy, Gd, La, Nd, Pr, Sm, Tb, Yb	$Ca_4Ag_{0.95}Mg$, Ln_4MMg (Ln = Ce, Dy, Gd, La, Nd, Pr, Sm, Tb, Yb, M = Co, Ir, Ru, Rh, Pd)
Ca	Hg	Ca_4Hg_9
Al	Cu	Cu_9Al_4, $Ni_{0.036}Cu_{0.69}Al_{0.274}$
Ga	Cu	Cu_9Ga_4
In	Dy, Er, Gd, Ho, Tm, Y, Tb, Nd, Pr, Ag, Au, Cu	Ln_4MIn (Ln = Dy, Er, Gd, Ho, Tm, Y, Tb, Nd, Pr, M = Ru, Rh, Ir), Ag_9In_4, Au_9In_4, Cu_9In_4
Fe	Hf, Zr, Ti	Hf_2Fe, Zr_2Fe, Ti_2Fe
Co	Ti, Hf, Zr	Ti_2Co, Hf_2Co, Zr_2Co
Ni	Ti, Zr, Sc	Ti_2Ni, Zr_4Ni_2Al, Sc_2Ni
Cu	Ti, Zr	Ti_2Cu, Zr_2Cu
Cd	Ce, Dy, Gd, Ho, La, Tb, Y	Ln_4MCd (Ln = Ce, Dy, Gd, La, Nd, Pr, Sm, Tb, M = Co, Rh, Ir, Ni, Pd, Pt, Ru)
Ru	Al	$RuAl_{12}$
Pd	Mg, Hf, Sc	Mg_2Pd, Hf_2Pd, Sc_2Pd
Ir	Hf, Sc, Zr	Hf_2Ir, $Sc_{11}Ru_4$, Zr_2Ir
Mn	Hf	Hf_2Mn
Os	Hf	Hf_2Os
Pt	Hf, Zr	Hf_2Pt, Zr_2Pt
Rh	Hf, Zr	Hf_2Rh, Zr_2Rh

3.5. Chemical Composition of γ-Brass Nanoclusters. The Hume–Rothery rules[16] imply that the structure of the γ-brass phases depends on the electron concentration. We emphasize that these rules cannot be directly applied to the subject matter of this paper since they deal with the overall structure of intermetallic compounds, whereas our approach concerns local configurations of atoms. However, one can expect that the topological and geometrical features of local configurations essentially predetermine the overall structure; hence some regularities in the chemical composition of the γ-brass nanoclusters can also be anticipated. To the best of our knowledge, nobody has performed such an overview that could also be useful to understand if the nanoclusters fused into the bulky structure of an intermetallic compound belong to the realm of chemistry or they are just geometrical and topological models. Below, we present the results of our analysis of the chemical composition of 702 crystallographically independent, i.e., not related by symmetry operations, 26-atom γ-configurations that exist in the 576 γ-brass-type phases, whose nanocluster models include such configurations as primary nanoclusters (in the Supporting Information, we give the full a reference list for 576 γ-brass-type phases).

The analysis shows that the 702 γ-configurations can include any lanthanide, Th, as well as almost any s-, p-, d-metal atom except Cs, W, Tc, Re. Only six metals form homoatomic nanoclusters M_{26} in seven structures: besides already mentioned Li_{26} nanoclusters in $Li_{13}Na_{29}Ba_{19}$[35] and $Li_{10}Pb_3$,[36] there are nanoclusters Al_{26} in $RuAl_{12}$,[54] Mn_{26} in Mn_3In,[55] Cu_{26} in $Cu_{40.5}Sn_{11}$,[17] Zn_{26} in $(FeNi)_{.99}Zn_{12.71}$,[56] and Cd_{26} in Cd_5Ni.[38] Nanoclusters A_4B_{22} with homoatomic shells are more numerous, most of them belong to the Gd_4RhIn structure type[30] (Table 3). One can spot at least two features of A_4B_{22} nanoclusters: (i) B atoms are often large lanthanides and (ii) the inner tetrahedron of the Fe triad atoms prefers to be surrounded by the atoms from the Ti group. More general conclusions with such a small sample are hardly possible.

More reliable regularities can be derived if we analyze the composition of the nested polyhedra. In Table S3 in the Supporting Information, we have collected the complete distributions of chemical elements among IT, OT, OH, and CO. One can see that some atoms occupy the first lines in all distributions, in particular, Mg, Al, Cu, and Zn. We could expect that these atoms should form homoatomic γ-brass nanoclusters and indeed Al, Cu, and Zn do it as was mentioned above. The compound containing nanocluster Mg_{26} has not been synthesized yet but perhaps it is the next candidate to the group of M_{26} nanoclusters.

In Figure 17, we have selected the elements that can form any nested polyhedron. Apparently, the electronic structure of the element influences the distribution much stronger than the atom size. In particular, independently of the atom size, all

Table 4. Occurrence of γ-Brass-Type Nanoclusters in Intermetallics

	no. of intermetallics in crystal system						
nanocluster (nested- polyhedron) configuration	triclinic	monoclinic	orthorhombic	tetragonal	trigonal	hexagonal	cubic
0@4@22 (γ-brass)	29	125	488	1590	987	2630	3525
0@4@26 (γ-brass)			1	18	4	2	115
0@4@30			1		1	18	51
0@6@28 (Ti_2Ni)		5	25	43	7	109	304
0@6@32							2
0@6@40 (Ti_2Ni)					1	12	159
0@8@26 (γ-brass)	7	18	22	215	42	8	2365
0@8@34 (γ-brass)	7	18	22	216	28	1	2468
0@8@38	7	24	33	605	45	39	2325
1@8@34 (BCC)	7	18	21	210	25	1	2351
1@14@40 (−CC γ-brass)							7
1@16@44 (α-Mn)					1		24

dx.doi.org/10.1021/ic4019713 | Inorg. Chem. 2013, 52, 13094–13107

elements of groups XI and XII as well as only three-valence lanthanides can participate in nested polyhedron of any type. On the other hand, unselected metals are also grouped in Figure 17 according to their participation in the nested

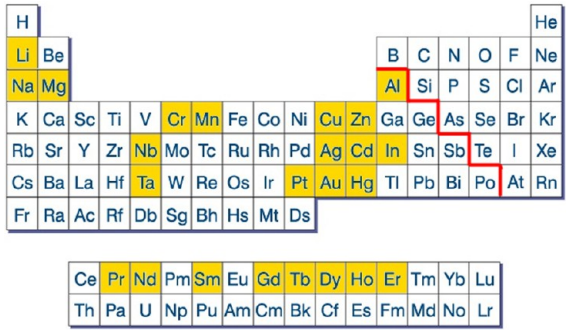

Figure 17. Elements highlighted by yellow occur in any type of nested polyhedra of γ-brass-type nanoclusters. The Zintl line is red.

polyhedra. Thus, all atoms of Fe triad as well as Ru, Rh, Pd, Os, Ir can form IT, OT, OH, but not CO; atoms of group IV can compose OT, OH and CO, but not IT; Mo, Cs, W, Tc, and Re do not participate in any nested polyhedron. At the same time, we have not found a simple relation (like the Hume−Rothery rules) between the electronic structure of atoms and their role in formation of the nested polyhedra.

A majority (56.2%) of the γ-brass-type nanoclusters has point symmetry T_d (the closest symmetry, T, was found only in one structure, Ag_2Hg_3);[57] however, lower symmetries C_1, C_s, C_{2v} or C_{3v} also occur. In all cases, the low-symmetry nanoclusters correspond to local configurations and do not form the structure of intermetallics according to the nanoclusters approach. Moreover, in all structures, the low-symmetry nanoclusters coexist with the nanoclusters of the T_d symmetry. Note that the elements not highlighted in Figure 17 can participate in the nested polyhedra of such low-symmetry nanoclusters; in this case, the polyhedron is formed by different atoms. For example, Fe, Co or Ni can combine with Zr to form CO of composition M_6Zr_6 or M_3Zr_9. Although four different elements can occupy vertices of four nested polyhedra in T_d γ-brass nanoclusters, we found only one structure, $(Zr_{0.75}Ti_{0.25})(Mn_{0.5}V_{0.5})_2$,[58] which includes four different elements. As was mentioned above, there are only seven (1.4%) pure (composed by one element) γ-brass nanoclusters, whereas the vast majority consist of two-element (58.8%) and three-element (39.8%) nanoclusters.

4. CONCLUSION

In this study, we have performed a detailed comparison of nanocluster models of the crystal structures of cubic intermetallics and found these nanoclusters closely related to each other. The results obtained establish topological relationships between the crystal structures of quite different intermetallics containing 26-atom γ-brass-type cluster thanks to transformations of atomic configurations. Robustness of the primary nanoclusters was proved by their frequent occurrence in intermetallics. Automated search for the primary nanoclusters and γ-configurations allowed us to find regularities in their chemical composition both within the nanoclusters approach (multishell structure) and within the nested-polyhedra model. Thus, nanoclusters can be considered as typical building blocks whose combinations can produce the whole variety of intermetallic architectures.

■ ASSOCIATED CONTENT

Supporting Information

We give tables in spreadsheet format to allow better reference: Table S1 contains the nanocluster models for all topological types where γ-brass-type clusters play a role of primary nanoclusters. Table S2 presents a comparison of nanocluster models with the other models published elsewhere. Table S3 list all references and formula compositions for 576 crystal structures that account for the 37 topological with primary nanoclusters containing γ-configuration listed in Tables S1 and S2. Table S4 lists the distributions of chemical elements among nested polyhedra IT, OT, OH, and CO of γ-brass-type nanoclusters. The set of zipped 28 gph files contains the information on γ-brass-type nanoclusters. This material is available free of charge via the Internet at http://pubs.acs.org.

■ AUTHOR INFORMATION

Corresponding Authors

*E-mail: blatov@samsu.ru. Phone: +7-8463345445. Fax: +7-8463345417.

*E-mail: davide.proserpio@unimi.it.

Notes

The authors declare no competing financial interest.

■ ACKNOWLEDGMENTS

The work was supported by Russian government (Grant 14.B25.31.0005). P.A.A., V.A.B., and G.D.I. are grateful to partial support of Russian Foundation for Basic Research for Grants 12-02-00493 and 13-07-00001. V.A.B. thanks the 2011/2012 Fellowship from Cariplo Foundation & Landau Network-Centro Volta (Como-Italy).

■ REFERENCES

(1) Pearson, W. B. *The Crystal Chemistry and Physics of Metals and Alloys*; Wiley−Interscience: New York, 1972.
(2) Hellner, E.; Koch, E. *Acta Crystallogr., Sect. A* **1981**, *37*, 1.
(3) Chabot, B.; Cenzual, K.; Parthé, E. *Acta Crystallogr., Sect. A* **1981**, *37*, 6.
(4) Nyman, H.; Andersson, S. *Acta Crystallogr., Sect. A* **1979**, *35*, 580.
(5) Lord, E. A.; Ranganathan, S. J. *Non-Cryst. Solids* **2004**, *334−335*, 121.
(6) Lord, E. A.; Mackay, A. L.; Ranganathan, S. *New Geometries for New Materials*; Cambridge University Press: Cambridge, U.K., 2006.
(7) Pankova, A. A.; Ilyushin, G. D.; Blatov, V. A. *Cryst. Rep.* **2012**, *51*, 1.
(8) Ilyushin, G. D. *Cryst. Rep.* **2004**, *49*, S5.
(9) Blatov, V. A.; Ilyushin, G. D.; Proserpio, D. M. *Inorg. Chem.* **2010**, *49*, 1811.
(10) Blatov, V. A.; Ilyushin, G. D.; Proserpio, D. M. *Inorg. Chem* **2011**, *50*, 5714.
(11) Blatov, V. A. *Struct. Chem.* **2012**, *23*, 955.
(12) Shevchenko, V. Ya.; Blatov, V. A.; Ilyushin, G. D. *Struct. Chem.* **2009**, *20*, 975.
(13) Ilyushin, G. D.; Blatov, V. A. *Acta Crystallogr., Sect. B* **2009**, *65*, 300.
(14) Berger, R. F.; Walters, P. L.; Lee, S.; Hoffmann, R. *Chem. Rev.* **2011**, *111*, 4522.
(15) Thimmaiah, S.; Miller, G. J. *Chem.—Eur. J.* **2010**, *16*, 5461.
(16) Mizutani, U. *Hume−Rothery Rules for Structurally Complex Alloy Phases*; CRC Press: Boca Raton, FL, 2011.
(17) Booth, M. H.; Brandon, J. K.; Brizard, R. Y.; Chieh, C.; Pearson, W. B. *Acta Crystallogr.* **1977**, *B33*, 30−36.
(18) Weber, T.; Dshemuchadse, J.; Kobas, M.; Conrad, M.; Harbrecht, B.; Steurer, W. *Acta Crystallogr., Sect. B* **2009**, *65*, 308.

(19) Dshemuchadse, J.; Jung, D. Y.; Steurer, W. *Acta Crystallogr., Sect. B* **2011**, *67*, 269.
(20) O'Keeffe, M.; Peskov, M. A.; Ramsden, S. J.; Yaghi, O. M. *Acc. Chem. Res.* **2008**, *41*, 1782.
(21) Ilyushin, G. D. *Struct. Chem.* **2012**, *23*, 997.
(22) Belin, C. H. E.; Belin, R. C. H. *J. Solid State Chem.* **2000**, *151*, 85.
(23) Bradley, A. J.; Jones, P. *J. Inst. Met.* **1933**, *51*, 131.
(24) Belsky, A.; Hellenbrandt, M.; Karen, V. L.; Luksch, P. *Acta Crystallogr., Sect. B* **2002**, *58*, 364. http://www.fiz-karlsruhe.de/icsd_home.html
(25) Villars, P.; Cenzual, K. *Pearson's Crystal Data—Crystal Structure Database for Inorganic Compounds (on CD-ROM)*; ASM International: Materials Park, OH, 2009.
(26) Tursina, A. I.; Nesterenko, S. N.; Noel, H.; Seropegin, Y. D. *Acta Crystallogr., Sect. E* **2005**, *61*, i99.
(27) Bie, H.; Mar, A. *J. Solid State Chem.* **2009**, *182*, 3131.
(28) Yurko, G. A.; Barton, J. W.; Parr, J. G. *Acta Crystallogr.* **1959**, *12*, 909.
(29) Szytula, A.; Bińczycka, H.; Todorović, J. *Solid State Commun.* **1981**, *38*, 41.
(30) Zaremba, R.; Rodewald, U. C.; Hoffmann, R. D.; Poettgen, R. *Monatsh. Chem.* **2007**, *138*, 523.
(31) Florio, J. V. *Acta Crystallogr.* **1952**, *5*, 449.
(32) Nyman, H. *J. Solid State Chem.* **1982**, *41*, 111.
(33) Johansson, A.; Westman, S. *Acta Chem. Scand.* **1970**, *24*, 3471.
(34) Thimmaiah, S.; Richter, K. W.; Lee, S.; Harbrecht, B. *Solid State Sci.* **2003**, *5*, 1309.
(35) Smetana, V.; Babizhetskyy, V.; Vajenine, G.; Simon, A. *Angew. Chem., Int. Ed.* **2006**, *45*, 6051.
(36) Rollier, M. A.; Arreghini, E. *Z. Kristallogr.* **1939**, *101*, 470–482.
(37) Pavlyuk, V.; Solokha, P.; Zelinska, O.; Paul-Boncour, V.; Nowik-Zajac, A. *Acta Crystallogr.* **2008**, *C64*, i50.
(38) Ljung, H.; Westman, S. *Acta Chem. Scand.* **1970**, *24*, 611.
(39) Sugiyama, K.; Saito, H.; Hiraga, K. *J. Alloys Compd.* **2002**, *342*, 148.
(40) Westin, L. *Chem. Scr.* **1971**, *1*, 127.
(41) Berger, R. F.; Lee, S.; Hoffmann, R. *Chem.—Eur. J.* **2007**, *13*, 7852.
(42) Samson, S.; Hansen, D. A. *Acta Crystallogr.* **1972**, *B28*, 930.
(43) Gribanov, A. V.; Seropegin, Yu.D.; Bodak, O. I.; Pavlyuk, V. V.; Aksel'rud, L. G.; Nikiforov, V. N.; Velikhovskii, A. A. *J. Alloys Compd.* **1993**, *202*, 133.
(44) Samson, S. *Acta Crystallogr.* **1972**, *B28*, 936.
(45) Brandon, J. K.; Brizard, R. Y.; Chieh, P. C.; McMillan, R. K.; Pearson, W. B. *Acta Crystallogr., Sect. B* **1974**, *30*, 1412.
(46) Bobev, S.; Sevov, S. C. *J. Am. Chem. Soc.* **2002**, *124*, 3359.
(47) Armbruster, M.; Lidin, S. *J. Alloys Compd.* **2000**, *307*, 141.
(48) Sichevich, O. M.; Bruskov, V. A.; Grin', Yu.N. *Sov. Phys. Cryst.* **1989**, *34*, 939.
(49) Biehl, E.; Deiseroth, H. J. *Z. Anorg. Allg. Chem.* **1999**, *625*, 1073.
(50) Gulay, L. D.; Schuster, J. C. *J. Alloys Compd.* **2003**, *360*, 137.
(51) Hornfeck, W.; Thimmaiah, S.; Lee, S.; Harbrecht, B. *Chem.—Eur. J.* **2004**, *10*, 4616.
(52) Lidin, S.; Jacob, M.; Larsson, A. K. *Acta Crystallogr.* **1994**, *C50*, 340.
(53) Solokha, P.; De Negri, S.; Pavlyuk, V.; Saccone, A. *Chem. Met. Alloys* **2009**, *2*, 39.
(54) Obrowski, W. *Metall. (Berlin)* **1963**, *17*, 108.
(55) Brandon, J. K.; Kim, H. S.; Pearson, W. B. *Acta Crystallogr., Sect. B* **1979**, *35*, 1937.
(56) Lidin, S.; Jacob, M.; Larsson, A. K. *Acta Crystallogr., Sect. C* **1994**, *50*, 340.
(57) Fairhurst, C. W.; Cohen, J. B. *Acta Crystallogr., Sect. B* **1972**, *28*, 371.
(58) Huot, J.; Akiba, E.; Iba, H. *J. Alloys Compd.* **1995**, *228*, 181.